Magnetic structure of hydrogen-induced defects on graphene

J. O. Sofo,[1] Gonzalo Usaj,[2] P. S. Cornaglia,[2] A. M. Suarez,[1] A. D. Hernández-Nieves,[2] and C. A. Balseiro[2]
[1]*Physics Department, Pennsylvania State University, University Park, Pennsylvania 16802, USA*
[2]*Centro Atómico Bariloche and Instituto Balseiro, CNEA, AR-8400 Bariloche, and CONICET, Argentina*
(Received 7 December 2011; published 6 March 2012)

Using density-functional-theory (DFT), Hartree-Fock, exact-diagonalization, and numerical-renormalization-group methods, we study the electronic structure of diluted hydrogen atoms chemisorbed on graphene. A comparison between DFT and Hartree-Fock calculations allows us to identify the main characteristics of the magnetic structure of the defect. We use this information to formulate an Anderson-Hubbard model that captures the main physical ingredients of the system while still allowing a rigorous treatment of the electronic correlations. We find that the large hydrogen-carbon hybridization puts the structure of the defect halfway between the one corresponding to an adatom weakly coupled to pristine graphene and that of a carbon vacancy. The impurity's magnetic moment leaks into the graphene layer where the electronic correlations on the C atoms play an important role in stabilizing the magnetic solution. Finally, we discuss the implications for the Kondo effect.

DOI: 10.1103/PhysRevB.85.115405 PACS number(s): 73.22.Pr, 81.05.ue, 73.20.Hb

I. INTRODUCTION

The unusual electronic and mechanical properties of graphene[1–6] triggered intense research activity after the first isolation of individual graphene sheets.[1,7,8] The anomalous charge-transport properties of pure graphene are a consequence of its particular sublattice symmetry that leads to a band structure with a pointlike Fermi surface and a linear dispersion close to the Fermi energy.[9] These properties are responsible for the peculiar low-energy excitations that correspond to massless Dirac fermions and for the long electron mean-free path.

The possibility of doping graphene with electrons or holes using external gates, which does not lead to a significant loss of mobility, allows the design of graphene-based devices. Another approach that is also viewed as a promising way to engineer the band structure and modify its electronic properties is the controlled adsorption of different types of atoms or molecules on graphene.[10–25] In particular, there has been increasing interest to incorporate magnetic effects in graphene to use graphene-based devices in spintronics.[14,19,26–30] There are already some advances in this direction, such as the injection of spin-polarized currents from ferromagnetic electrodes.[26,31,32] An alternative route is the generation of magnetic defects using, for example, adatoms, vacancies, or edges. Hydrogen (H) impurities and carbon (C) vacancies are among the simplest and most studied pointlike magnetic defects.[33–38]

The problem of H atoms chemisorbed on graphene has been studied by several groups.[11,16,17,23,30,39,40] It is known that H impurities are adsorbed on top of a C atom, forming a covalent bond and locally distorting the honeycomb lattice. There is an increasing consensus that H adatoms acquire a magnetic moment, therefore behaving as magnetic impurities. A simple picture used to describe H on graphene is based on the Anderson model in which the localized 1*s* H orbital is hybridized with the graphene extended states. The intra-atomic Coulomb repulsion at the 1*s* orbital, together with the graphene pseudogap, favors the existence of a local moment at the H impurity.[14,19]

The case of C vacancies is quite different. In the ideal case in which the lattice remains undistorted after the removal of a C atom,[27] there is a reduction of the coordination number of the three neighboring atoms that generates a resonant state at the pseudogap.[41] The existence of this resonance together with the intra-atomic Coulomb repulsion at the C orbitals naturally leads to the formation of a magnetic moment. This simple picture is consistent with the observation of magnetic, Kondo-like correlations in irradiated samples[42] and enlightens the role of the on-site Coulomb interaction in graphene (from hereon denoted as U_C). The parameter U_C has been estimated to be on the order of a few electronvolts.[43]

A realistic description of the impurities on graphene should then include the effects of the electronic correlations in both the impurity and the C orbitals by means of an Anderson-Hubbard-like model. Such a model can extrapolate between two different limits. (i) For a small value of the hybridization between the impurity and C orbitals, a magnetic moment that is mainly localized at the impurity orbital can be stable, and (ii) for a large hybridization, bonding and antibonding states are shifted away from the low-energy region. The effect of these shifts is to effectively remove the p_z orbital of the hybridized carbon atom from the Fermi energy generating a vacancylike defect with a magnetic moment localized at the C atoms.

As we will discuss below in detail, we find that the case of a H adatom on graphene is halfway between these two limiting cases. We show that the H impurity creates a defect with a complex magnetic structure for which a spin $S = \frac{1}{2}$ is localized in a linear combination of the H and the neighboring C orbitals, showing some of the properties of the vacancylike defect.

The paper is organized as follows. In Sec. II we revisit the density functional theory (DFT) for diluted H on graphene and use the results as a guide to estimate realistic effective parameters. In Sec. III we present an Anderson-Hubbard model, and its Hartree-Fock solution is compared with DFT results. In Sec. IV we show that the results can be interpreted in terms of an effective model of a H-C's cluster embedded in an effective medium and use the numerical renormalization group (NRG) to analyze the stability of the magnetic solution. Finally, a summary and our conclusions are presented in Sec. V.

II. DFT RESULTS

We consider a graphene layer with a low concentration of H atoms. We calculate the spin-dependent electronic structure of systems with a unit cell of N C atoms and one H atom for which N ranges between 32 and 72. Our DFT calculations were done with a plane-wave basis as implemented in the VASP code,[44] and the cutoff energy was set to 400 eV. The core electrons were treated with a frozen-core projector-augmented-wave (PAW) method.[45,46] The frozen-core pseudopotential for carbon used a core radius for the s partial waves of 1.20 a.u. and 1.5 a.u. for the p channel. All partial waves for H where treated with a cutoff radius of 1.10 a.u. We use the Perdew-Burke-Ernzerhof (PBE)-generalized gradient approximation to treat the exchange and correlations.[47,48] To correct for the dipole moment generated in the cell and to improve convergence with respect to the periodic cell size, monopole and dipole corrections were considered.[49,50]

Figure 1 shows the relaxed structure of a supercell of 72 C atoms containing one H adatom. After minimizing the total energy with respect to the coordinates of all atoms in the unit cell, we find a H-induced distortion consisting of a puckering of the hybridized carbon atom. The distortion is due to the modification of the electronic structure of the C atom bonded with the H adatom that changes from an sp^2 configuration to an sp^3-like configuration after the hybridization with the H orbital. In the following, we use the label C_0 for the C atom directly bonded to the H impurity. C_0 is represented by a green (light gray) sphere in Fig. 1. The second-nearest-neighbor C atoms are represented by red (dark gray) spheres and are labeled as C_n with $n = 1,2,3$.

Partial densities of states (PDOSs) are calculated using a projector scheme provided in the PAW implementation of VASP4.6 when LORBIT = 11. The PDOS corresponding to the H atom shows the existence of a spin-split resonant state close to the Fermi level [see Fig. 2(a)]. This induces a total magnetic moment of $\approx 0.49\ \mu_B$/cell localized around the impurity. The covalent bond with the H induces a spin polarization in the surrounding C atoms. The spin polarization is small in the nearest C atom (C_0) as shown in Fig. 2(b) where there is only a small spin-polarized peak close to the Fermi level. The magnetic moment is larger at the second-nearest-neighbor C atoms (C_n) as can be appreciated from the strong spin polarization of the p_z orbitals of these atoms [see Fig. 2(c)].

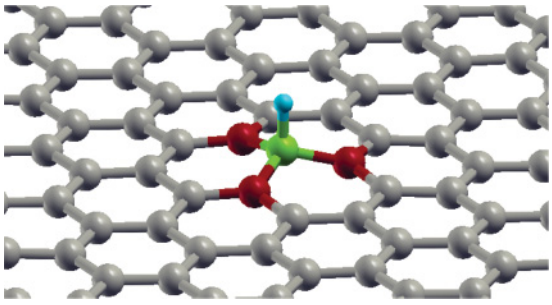

FIG. 1. (Color online) Three-dimensional view of a supercell containing 72 C atoms (large spheres) and one H impurity (small sphere) on top of a C atom (C_0) represented by a green (light gray) sphere. The second nearest-neighbor C atoms (C_n with $n = 1,2,3$) are represented by red (dark gray) spheres.

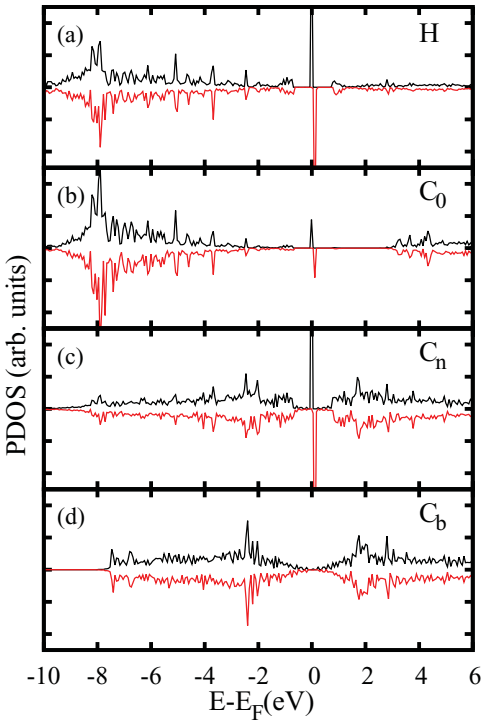

FIG. 2. (Color online) Partial densities of states for the undoped case projected on (a) the H atom, (b) the p_z orbitals of the nearest-neighbor carbon atom (C_0), (c) one of the second-nearest-neighbor carbon atoms (C_n), and (d) a C atom located far from the adatom. For each case, both the majority- and minority-spin PDOSs are plotted. A clear spin-polarized resonant state near the Fermi level E_F is observed in (a) and (c).

The spin polarization induced by the H adatom on the graphene layer tends to decrease at large distances from the absorption point, and far from the H adatom the PDOS corresponding to the p_z orbitals of the C atoms [see Fig. 2(d)] shows a Dirac point similar to that of the behavior of the C atoms in pristine graphene.

The H adatom induces a magnetic moment and charge redistribution on the surrounding carbon atoms that can be analyzed by monitoring the atomic charge and magnetization as a function of the distance between the H atom and the graphene plane (R). This is shown in Fig. 3. The vertical dashed line marks the equilibrium position. The charge of the H atom increases, and its magnetic moment decreases as it approaches the graphene sheet as shown in Figs. 3(a) and 3(b). The opposite occurs for the second-nearest-neighbor C_n atoms (red short-dashed lines) in Figs. 3(c) and 3(d), i.e., the charge of the C_n atoms decreases while the magnetization increases as the H atom approaches the graphene sheet. A different behavior can be observed at the absorption site, the C_0 atom. In this case, the charge shows a minimum and the absolute value of the magnetization a maximum close to the equilibrium position.

Far from the absorption site, the perturbation induced by the H atom is smaller and alternates its magnitude between sublattices; it is larger on the sublattice corresponding to the C_n atoms. For example, the charge of the third nearest neighbors [C_{nn} atoms in Fig. 3(c)] is almost independent of

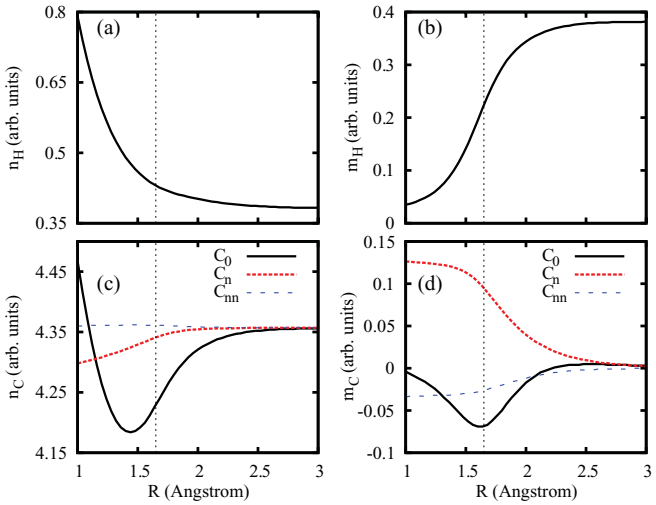

FIG. 3. (Color online) Charge and magnetization of the most relevant atoms as a function of the distance R between the H atom and the graphene sheet. The equilibrium position of the adatom is indicated by a vertical dashed line. Notice how the charge (magnetization) of the H atom increases (decreases) as it approaches the graphene sheet. The opposite occurs for the C_n atoms (red short-dashed lines). Both the charge and the magnetization of the C_0 atom have a minimum close to the equilibrium position.

the position of the adatom whereas the magnetization of these atoms only changes slightly compared with the changes in the magnetization of the C_n atoms [compare the red short-dashed and blue dashed lines in Fig. 3(d)]. This shows that the H atom generates a charge redistribution mostly on the same sublattice of the adsorption site and Êpredominantly at the neighboring C atoms, those that were highlighted with different colors in Fig. 1. As we will see in the next sections, the behavior of the system can be described by a simple model that takes into account the *e-e* correlations only in these atoms and connects them with the rest of the graphene lattice described with a simpler approximation.

As was found recently for the case of fluorine adatoms,[51] the nature of the chemical bonding of adatoms on graphene can change strongly with electron and hole doping. When graphene is electron doped, the C_0 atom bonded to the F atom retracts back to the graphene plane, and for high doping its electronic structure corresponds to nearly a pure sp^2 configuration (see Ref. 51 for details). The situation is different for the electron doping of graphene with H impurities. To simulate electron doping, we add one electron per unit cell. The extra charge is compensated with a uniform charge background. The results obtained are shown in Fig. 4. The most important difference between Figs. 2 and 4 is the absence of spin polarization in the system after electron doping. As we can see, a similar electronic structure with well defined peaks at the Fermi level is observed, but neither the H atom nor the C_0 or C_n atoms show spin polarization [see Figs. 4(a)–4(c)]. This dependence between gate doping and the magnetic moment highlights the delicate interplay between electron correlations and localization in graphene with chemisorbed adatoms. In the following, we use our DFT results as a guide to formulate a theory that goes beyond the mean-field level.

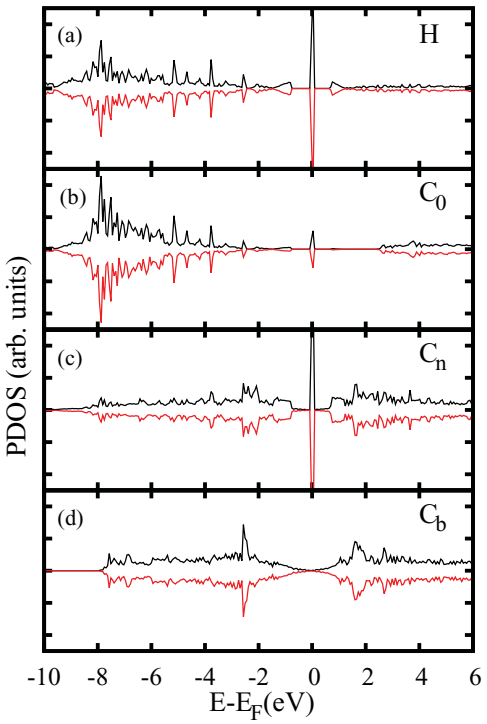

FIG. 4. (Color online) Same as Fig. 2 but doped with an extra electron in the unit cell. Notice the absence of spin polarization in the system after electron doping.

III. ANDERSON-HUBBARD MODEL

In order to interpret the DFT results and give a more physical picture of the magnetic structure of the defect, we use a simple Anderson-Hubbard (AH) model given by

$$\hat{\mathcal{H}} = \hat{\mathcal{H}}_{\text{graph}} + \hat{\mathcal{H}}_{\text{imp}} + \hat{\mathcal{H}}_{\text{hyb}}, \tag{1}$$

where $\hat{\mathcal{H}}_{\text{graph}}$ describes the π bands of the graphene sheet as

$$\hat{\mathcal{H}}_{\text{graph}} = -\sum_{\langle i,j\rangle\sigma} t_{ij} c^{\dagger}_{i\sigma} c_{j\sigma} + U_C \sum_i \left(\hat{n}_{i\uparrow} - \frac{1}{2}\right)\left(\hat{n}_{i\downarrow} - \frac{1}{2}\right). \tag{2}$$

Here, $c^{\dagger}_{i\sigma}$ creates an electron with spin σ at site i of the graphene lattice, the first sum runs over the nearest neighbors, U_C is the Coulomb repulsion in the carbon atoms, and $\hat{n}_{i\sigma} = c^{\dagger}_{i\sigma} c_{i\sigma}$ is the number operator of site i. The H impurity, which is bounded to the C_0 atom located at site $i = 0$, is described by

$$\hat{\mathcal{H}}_{\text{imp}} = \sum_{\sigma} \varepsilon_H h^{\dagger}_{\sigma} h_{\sigma} + U_H h^{\dagger}_{\uparrow} h_{\uparrow} h^{\dagger}_{\downarrow} h_{\downarrow}, \tag{3}$$

where $h^{\dagger}_{\sigma}$ creates an electron with spin σ at the $1s$ orbital of the H impurity with energy ε_H and intra-atomic Coulomb repulsion U_H. The impurity-graphene interaction includes a one-body hybridization V and a distortion-induced shift of the

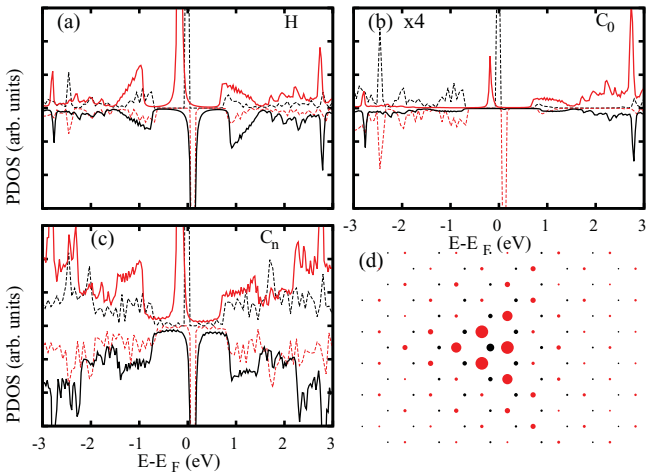

FIG. 5. (Color online) Comparison between the DFT PDOS (dashed line) projected onto the p_z orbitals and the Hartree-Fock (solid line) results obtained with the full AH model. In both cases we use a 72-C-atom unit cell. (d) The spatial distribution of the magnetization on the C atoms obtained with the AH model for a unit cell of 288 C atoms in which finite-size effects are negligible.

C_0 carbon energy ε_0 as

$$\hat{\mathcal{H}}_{\rm hyb} = \varepsilon_0 \hat{n}_0 - V \sum_{\sigma} (c^{\dagger}_{0\sigma} h_{\sigma} + h^{\dagger}_{\sigma} c_{0\sigma})$$

with $\hat{n}_0 = c^{\dagger}_{0\uparrow} c_{0\uparrow} + c^{\dagger}_{0\downarrow} c_{0\downarrow}$. In what follows we assume that the hopping-matrix elements t_{ij} with $i,j \neq 0$ are all equal to $t = 2.8$ eV while $t_{0j} = t_{j0}$ is reduced by the distortion. The energy of the hybridized carbon orbital is given by $\varepsilon_0 = A^2(\varepsilon_s - \varepsilon_p)$, where $\varepsilon_s \sim -8$ eV and $\varepsilon_p \equiv 0$ are the energies of the s and p carbon orbitals, respectively, while A is a constant that parametrizes the deformation of the sp^2 bonding of C_0.[15] This expression interpolates between $A = 0$ for the sp^2 and $A = \frac{1}{2}$ for the sp^3 configurations. From the DFT results for the PDOS of a H far from the graphene surface, we obtain that $\varepsilon_H \sim -1.4t$ and $U_H \sim 2.8t$ while we set $U_C = t$. Guided by the DFT results, we take $t_{0j} = t_0 = 0.6t$, $\varepsilon_0 = -0.7t$, and $V = 2t$.

Figure 5 shows a comparison of the DFT results for the PDOS projected onto the p_z orbitals with those obtained with the AH model within the Hartree-Fock (HF) approximation. In both cases we used a cell of 72 C atoms to facilitate the comparison. There is a good qualitative agreement between both methods, indicating that the chosen effective AH parameters are adequate for capturing the relevant aspects of the problem; it should be emphasized that we do not intend to fit the parameters but instead find a reliable range of values for them. The overall qualitative agreement includes some features related to the finite size of the cell as, for example, the appearance of gaplike and sharp-peak structures. This is a consequence of the interference effects introduced by the periodic array of impurities (all in the same sublattice). Within our model, such an effect can be eliminated without much numerical effort by increasing the size of the unit cell. Figure 5(d) shows the spatial profile of the magnetization on a cell containing 288 C atoms, which shows a triangular symmetry characteristic of an isolated impurity.

A. Minimal Anderson-Hubbard model

The AH model presented above can be further reduced to a much simpler model that still captures the relevant aspects of the problem, allows us to consider a single isolated impurity, greatly reduces the numerical work, and reproduces to an excellent accuracy the results of the full HF approach obtained with large unit cells. We first note that within the HF approximation, the presence of the H impurity generates a small charge redistribution mainly on its neighboring C atoms, namely, in the C_0 atom and the three next-nearest neighbors C_n with $n = 1,2,3$ (see Fig. 1). Therefore, it is sufficient to limit ourselves to consider a small cluster embedded in an effective medium in which the energies of the p_z orbitals are fixed and the occupation numbers are solved self-consistently in the cluster. This approximation is numerically simpler as the self-consistent equations can be expressed in terms of the integrals of analytical functions. Moreover, based on this approximation, the reduced Hamiltonian can be treated using more powerful numerical tools like exact diagonalization or the numerical renormalization group presented in the next section.

To illustrate the procedure, let us first consider the one-body part of $\hat{\mathcal{H}}$. Due to the hexagonal structure of the lattice, the C_0 atom only couples to the symmetric combination of the p_z orbitals of its nearest-neighbor carbon atoms (C_n). We denote that state as $|\triangle\rangle$ and the corresponding fermionic operator as $c^{\dagger}_{\triangle\sigma} = \sum_n c^{\dagger}_{n\sigma}/\sqrt{3}$, where $n = 1,2,3$ labels the C_n atoms. (We will also refer to this state as $C_{\triangle}$.) The other two orthogonal linear combinations of the C_n p_z orbitals, denoted by $|\pm\rangle$, are not directly coupled to C_0. Furthermore, because of the symmetry of the hexagonal lattice, the states $|\triangle\rangle$ and $|\pm\rangle$ are not coupled by the rest of the lattice either. As a result, the one-body terms of $\hat{\mathcal{H}}$ can be separated into three decoupled parts as is schematically shown in Fig. 6.

Hence, for calculating the properties of the H impurity, the C_0 atom, and $C_{\triangle}$, it is sufficient to consider a reduced Hamiltonian for the reduced system (see Fig. 6) and include the rest of the lattice as an effective self-energy $\Sigma_{\triangle}(\omega)$; the calculation is presented in the Appendix. More explicitly, the one-body Green function of the reduced system can be written

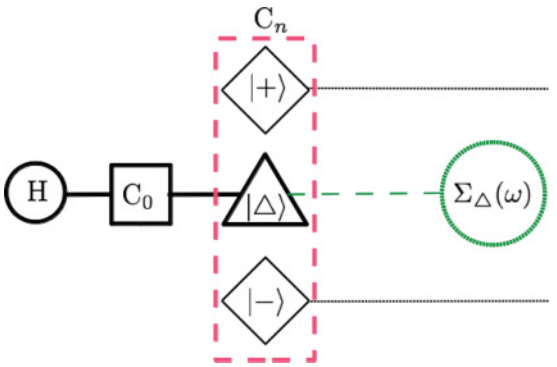

FIG. 6. (Color online) Schematic representation of the MAHM. The H impurity, the C_0 atom, and the state $|\triangle\rangle$ are treated exactly while the rest of the C atoms are treated as a noninteracting reservoir represented by the self-energy $\Sigma_{\triangle}(\omega)$. The capacitive coupling to the $|\pm\rangle$ states is taken into account only through a mean-field approximation (see text).

as $\boldsymbol{G}(\omega) = [\omega \boldsymbol{I} - \boldsymbol{\mathcal{H}}_r(\omega)]^{-1}$ with

$$\boldsymbol{\mathcal{H}}_r(\omega) = \begin{pmatrix} \varepsilon_H & V & 0 & 0 & 0 \\ V & \varepsilon_0 & \sqrt{3}t_0 & 0 & 0 \\ 0 & \sqrt{3}t_0 & \varepsilon_\triangle + \Sigma_\triangle(\omega) & 0 & 0 \\ 0 & 0 & 0 & \varepsilon_+ + \Sigma_+(\omega) & 0 \\ 0 & 0 & 0 & 0 & \varepsilon_- + \Sigma_-(\omega) \end{pmatrix}, \tag{4}$$

where we have included the possibility that the C_n atoms have a different energy than the rest of the C atoms of the graphene lattice (and included the $|\pm\rangle$ states for completeness). So far, this is an exact procedure. The addition of the Coulomb interactions U_H and U_C *only* in C_0 can still be treated in a similar way, provided we use the appropriate method, as the rest of the system remains a noninteracting fermionic bath, and it can still be represented by $\Sigma_\triangle(\omega)$. This is no longer true when interactions are included in the rest of the C atoms. We will argue, however, that for a qualitative understanding it is sufficient, and important, to take into account the U_C interaction *only on* C_0 and the C_n ($n = 1,2,3$) atoms. We will refer to this model as the minimal Anderson-Hubbard model (MAHM).

At the level of the HF approximation, the Coulomb repulsion $U_C \sum_{i=1,2,3}(\hat{n}_{i\uparrow} - \frac{1}{2})(\hat{n}_{i\downarrow} - \frac{1}{2})$ shifts the energy of the states $|\triangle\rangle$ and $|\pm\rangle$, preserving the form of the effective Hamiltonian $\boldsymbol{\mathcal{H}}_r(\omega)$ for each spin projection and then the propagators. The spin-dependent self-consistent Green function $\tilde{\boldsymbol{G}}_\sigma$ of the system is obtained from Eq. (4) with the self-consistent energies $\tilde{\varepsilon}_H^\sigma = \varepsilon_H + U_H(\langle \hat{n}_{H\bar{\sigma}} \rangle - \frac{1}{2})$, $\tilde{\varepsilon}_0^\sigma = \varepsilon_0 + U_C(\langle \hat{n}_{0\bar{\sigma}} \rangle - \frac{1}{2})$, and

$$\tilde{\varepsilon}_\triangle^\sigma = \varepsilon_\triangle + U_C\left(\frac{\langle \hat{n}_\triangle^{\bar{\sigma}} \rangle + \langle \hat{n}_+^{\bar{\sigma}} \rangle + \langle \hat{n}_-^{\bar{\sigma}} \rangle}{3} - \frac{1}{2}\right) \tag{5}$$

with $\bar{\sigma} = -\sigma$. We have tested the validity of the MAHM by comparing the PDOSs of the H, the C_0, and the C_n atoms with those obtained with the full model that includes the U_C interactions everywhere. The agreement between both approaches is excellent, provided the unit cell used in the latter case is large enough for the finite-cell-size effects to be negligible. It is also worthwhile to emphasize that the MAHM leads to a magnetic structure similar to the one shown in Fig. 5(d), indicating that much of the observed antiferromagnetic structure is related to Friedel oscillations.

It is interesting to compare the results of the MAHM with those of DFT. For that purpose, we plot in Fig. 7(a) the magnetization of the H, C_0, and C_n atoms as a function of the hybridization V for two different values of ε_H. (This is equivalent to plotting it as a function of the H–C_0 distance if an exponential dependence of V is assumed.) These results should be compared with those in Fig. 3. We clearly see that the MAHM is able to capture the most relevant features of the DFT results, namely, that the magnetic state of the impurity is somewhere in between a pure adatom state ($V \ll t$) where the magnetization is mainly localized at the H atom and a vacancy state ($V \to \infty$) where a substantial amount of magnetization has been transferred to the C_n atoms (mainly dominated by the $|\triangle\rangle$ state). For a quantitative comparison of the results, we have to consider the fact that in the DFT approach the lattice is relaxed for each H-graphene distance, and consequently, other parameters, such as ε_0 and t_0, also depend on the distance. Figure 7(b) shows the same parameters but in the absence of the *e*-*e* interaction on the C atoms. Clearly, the U_C interaction plays an important role in the case of large V (the vacancylike state), being responsible for the reentry behavior observed in Fig. 7(a).

Before discussing the effect of the interactions beyond the HF approximation, we note that for $\omega \to 0$, the self-energy $\Sigma_\triangle(\omega) \sim \alpha\omega \ln|\omega| - i\sqrt{3}\,|\omega|$ and the spectral density of the $|\triangle\rangle$ state presents a divergence at the Dirac point $-\mathrm{Im}(g_\triangle) = -\mathrm{Im}\{1/[\omega - \Sigma_\triangle(\omega)]\}$. This is precisely the vacancy state (projected onto the $|\triangle\rangle$ state) that has been extensively discussed in the literature.[41,52] This singular density of states is what makes the $|\triangle\rangle$ state unstable against the formation of a localized magnetic moment when the interactions are included. Conversely, the $\Sigma_\pm(\omega)$ self-energies diverge at the Dirac point, and the spectral densities of the $|\pm\rangle$ states show a pseudogap at low energies (see the Appendix). In view of this, one can expect that the main role of the U_C interaction at

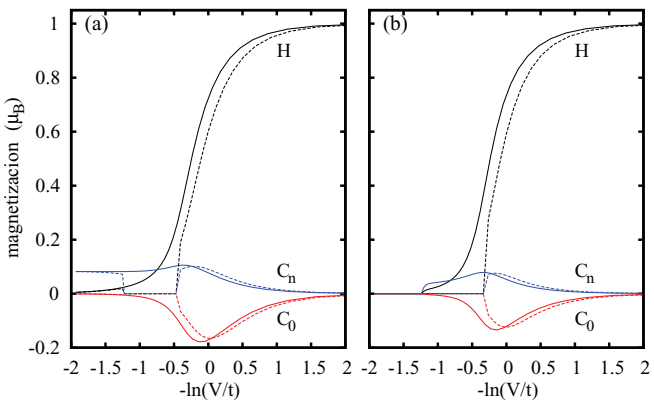

FIG. 7. (Color online) Site magnetization as a function of the hybridization V between the H and C_0 atoms obtained within the MAHM for two different values of ε_H: $\varepsilon_H = 1.29t$ (solid lines) and $\varepsilon_H = 0.7t$ (dashed lines) and for (a) $U_C = t$ and (b) $U_C = 0$. Notice that the simple model is able to capture the general trend of the spatial distribution of the magnetic structure (compare with Fig. 3). The presence of U_C not only induces some magnetization of the C_n atoms for large V but can also lead to reentry behavior of the magnetization.

low energies will manifest through the weakest coupled state $|\triangle\rangle$. Therefore, we only keep the $U_C/3(\hat{n}_{\triangle\uparrow}-\frac{1}{2})(\hat{n}_{\triangle\downarrow}-\frac{1}{2})$ part of the interaction between the C_n ($n=1,2,3$) atoms in what follows and neglect the rest.

Under these assumptions the reduced Hamiltonian (MAHM) describes a correlated three-site cluster, given by the H, the C_0, and the $|\triangle\rangle$ orbitals, embedded in an effective medium with a pseudogap described by $\Sigma_\triangle(\omega)$; the mean-field-charge interaction between the $|\triangle\rangle$ and the $|\pm\rangle$ orbitals that tends to keep the charge neutrality of the $|\triangle\rangle$ state can be included through an effective site energy $\bar{\varepsilon}_\triangle$. In the next section we analyze the properties of this model.

IV. EXACT-DIAGONALIZATION AND NRG RESULTS

The reduced Hamiltonian has the form

$$\hat{\mathcal{H}}_R = \hat{\mathcal{H}}_{\text{cluster}} + \hat{\mathcal{H}}_{\text{band}} + \hat{\mathcal{H}}_{\text{hyb}}, \tag{6}$$

where

$$\begin{aligned}\hat{\mathcal{H}}_{\text{cluster}} &= \varepsilon_H \hat{n}_H + U_H h^\dagger_\uparrow h_\uparrow h^\dagger_\downarrow h_\downarrow + \varepsilon_0 \hat{n}_0 \\ &+ U_C\left(\hat{n}_{0\uparrow}-\frac{1}{2}\right)\left(\hat{n}_{0\downarrow}-\frac{1}{2}\right) \\ &+ \bar{\varepsilon}_\triangle \hat{n}_\triangle + \frac{U_C}{3}\left(\hat{n}_{\triangle\uparrow}-\frac{1}{2}\right)\left(\hat{n}_{\triangle\downarrow}-\frac{1}{2}\right) \\ &- V\sum_\sigma (c^\dagger_{0\sigma} h_\sigma + h^\dagger_\sigma c_{0\sigma}) \\ &- \sqrt{3}t_0 \sum_\sigma (c^\dagger_{\triangle\sigma} c_{0\sigma} + c^\dagger_{0\sigma} c_{\triangle\sigma})\end{aligned} \tag{7}$$

and $\hat{\mathcal{H}}_{\text{band}}$ and $\hat{\mathcal{H}}_{\text{hyb}}$ describe a band with a pseudogap at the Dirac point and the coupling to the $|\triangle\rangle$ state, respectively:

$$\hat{\mathcal{H}}_{\text{band}} = \sum_{\nu\sigma} \varepsilon_\nu f^\dagger_{\nu\sigma} f_{\nu\sigma}, \tag{8}$$

$$\hat{\mathcal{H}}_{\text{hyb}} = \sum_{\nu\sigma} t_\nu (f^\dagger_{\nu\sigma} c_{\triangle\sigma} + c^\dagger_{\triangle\sigma} f_{\nu\sigma}), \tag{9}$$

which can be rewritten as

$$\hat{\mathcal{H}}_{\text{hyb}} = \sqrt{2}t \sum_\sigma (f^\dagger_{0\sigma} c_{\triangle\sigma} + c^\dagger_{\triangle\sigma} f_{0\sigma}), \tag{10}$$

where $f^\dagger_{0\sigma} = \frac{1}{\sqrt{2}t}\sum_\nu t_\nu f_{\nu\sigma}$ creates an electron on a symmetric combination of H's third-nearest-neighbor C atoms.

It is instructive to start the analysis by looking at the many-body states of the isolated cluster. For undoped graphene ($\mu=0$), we take $\bar{\varepsilon}_\triangle = 0$, $U_H \sim 3t$, and $U_C = t$ as in the previous sections but take $\varepsilon_0 = 0$ in what follows to simplify the analysis. (Taking $\varepsilon_0 \neq 0$ introduces an electron-hole asymmetry which is not relevant at this point.)

We diagonalize $\hat{\mathcal{H}}_{\text{cluster}}$ in the different charge sectors for different values of ε_H and V. Figure 8 shows the regions of stability of the different charge states in the $[\varepsilon_H, V]$ plane. For $\varepsilon_H \sim -U_H/2$, the ground state is always a three-particle state with spin $S=1/2$. The region of stability of the magnetic states as a function of ε_H shows a narrowing for $V \sim 2t$. For $V < 2t$, the magnetic moment is localized mainly at the H orbital while for $V > 2t$ it is transferred to the $|\triangle\rangle$ state. Note that as the hybridization increases, the spin is transferred

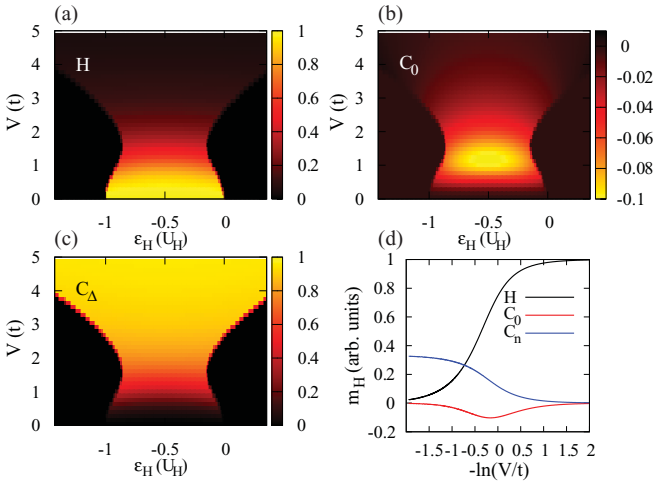

FIG. 8. (Color online) Color maps showing the magnetization of the H, C_0, and $C_\triangle$ atoms as a function of the orbital energy of the H atom, ε_H, and the adatom hybridization V as obtained from the exact diagonalization of $\hat{\mathcal{H}}_{\text{cluster}}$. (d) The magnetization for $\varepsilon_H = -U_H/2$. (Note that here the magnetization of C_n is plotted.)

directly from the H atom to the $|\triangle\rangle$ orbitals in agreement with the DFT and HF results. This is more clearly seen in Fig. 8(d) where the magnetization of the H, C_0, and C_n atoms is plotted as a function of $\ln(V/t)$ for $\varepsilon_H = -U_H/2$. In agreement with the previous results, the magnetic moment is transferred to the C orbitals as the hybridization increases.

From these exact results we can now calculate the Kondo coupling constant J. This is done in the standard way, eliminating high-energy states of the cluster through a Schrieffer-Wolff transformation[53] to get

$$J = 2t^2 \sum_{\nu\sigma} \frac{\langle\Uparrow|c^\dagger_{\triangle\sigma}|\nu\rangle\langle\nu|c_{\triangle\sigma}|\Downarrow\rangle + \langle\Uparrow|c_{\triangle\sigma}|\nu\rangle\langle\nu|c^\dagger_{\triangle\sigma}|\Downarrow\rangle}{E_\nu - E_\Uparrow}, \tag{11}$$

where $|\sigma\rangle$ ($\sigma = \Uparrow, \Downarrow$) is the degenerate ground state of the cluster with energy $E_\Uparrow = E_\Downarrow$ and the $|\nu\rangle$ are excited states. Note that in the absence of electron-hole symmetry in the cluster, there will also be a local potential scattering for the conduction electrons due to the cluster.

Figure 9(a) shows the J coupling in the $[\varepsilon_H, V]$ plane while Fig. 9(b) shows its dependence on V for different values of ε_H. For small $V \ll t$, the magnetic moment, which is mainly localized on the H atom, is weakly coupled to the graphene sheet, and the Kondo coupling is small. For a fixed V, the Kondo coupling increases as ε_H approaches the charge-degeneracy lines where perturbation theory fails, and so J diverges due to vanishing denominators in Eq. (11). For large $V > 2t$, the bond between the H atom and the C_0 atom is strong enough to effectively decouple both atoms from the rest of the system. The magnetic moment is transferred to the $|\triangle\rangle$ state, and the Kondo coupling becomes V independent. In the large-V limit it is simply given by $J(V\to\infty) = 8t^2/U_\triangle = 24t$.

We complete the analysis by coupling the cluster to the rest of the graphene layer, providing the hybridization $\Gamma_\triangle \sim \sqrt{3}|\omega|$ at low energies. In the parameter region where the cluster is

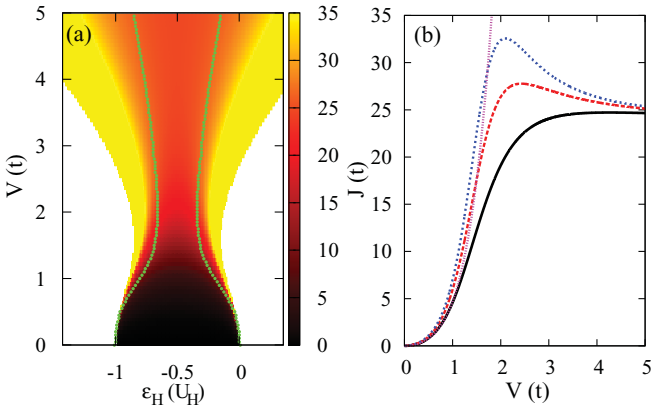

FIG. 9. (Color online) Kondo coupling constant J estimated from the exact diagonalization of the MAHM cluster (a) as a function of ε_H and V and for the same parameters as in Fig. 8. In the white-color regions there is no magnetic moment on the cluster. (b) J as a function of V for three different values of ε_H: $-U_H/2$ (solid line), $-0.8t$ (dashed line), and $-0.7t$ (short-dashed line). The case $U_C = 0$ (dotted line) is included for comparison.

magnetic, we end up with a pseudogap Kondo problem.[19,54–63] In this model, for an electron-hole symmetric impurity, the magnetic moment of the impurity (the cluster in the present case) remains unscreened even at zero temperature. For the electron-hole asymmetric situation, the magnetic moment can be screened only if the Kondo coupling is larger than a critical coupling J_c on the order of the bandwidth.[54,55,64] We calculated the stability of the magnetic moment in the cluster when it is coupled to the rest of the system. We used the NRG[65,66] with a pseudogapped density of states and a Fermi velocity chosen to reproduce the effect of $\Sigma_\triangle(\omega)$.

The solid line in Fig. 9(a) shows the NRG results for the stability region of the total magnetic moment on the cluster at zero temperature, that is, the cluster's magnetic moment is nonzero only in the region enclosed by the solid lines. We observe that the coupling to the rest of the system reduces the parameter area where the magnetic moment is stable at zero temperature. (A similar effect is observed in the Hartree-Fock solution.) For $V \lesssim 2t$, the magnetic moment is mainly localized on the H atom, and it is screened when the Kondo coupling reaches a critical value of $\sim 10t$. (This unconventional screening is associated to a change of the cluster's charge.[62]) For larger values of V, the magnetic moment is localized on the $|\triangle\rangle$ state. At finite but large ($>2t$) values of V, the critical coupling increases with increasing V. This is due to the fact that in the present model, if $V \to \infty$ the magnetic impurity becomes electron-hole-symmetric for any value of ε_H, and the magnetic moment remains unscreened for any value of J.

It is worth mentioning that in the doped case the magnetization maps of Fig. 8 are modified.[14] For $V \gtrsim 2t$, the magnetic-moment-stability region narrows and shifts, being centered around a line given by $V^2 \sim a\varepsilon_H + b$. This shows that the impurity state is much more sensitive to doping in the vacancylike regime than in the low-V regime where the magnetic moment is localized at the H atom. Therefore, a realistic H-induced defect on graphene would be more sensitive to doping than what one would expect from the usual Anderson-like model for an impurity on pristine graphene. A detailed study of this effect will be presented elsewhere.

V. SUMMARY AND CONCLUSIONS

We have combined a DFT description of diluted H impurities on graphene with tight-binding and effective models to describe the magnetic structure of a H-induced defect. The DFT approach provides a realistic picture of the structural distortions around the adsorbed H atom and predicts a magnetic moment localized in the neighborhood of the adatom. Additionally, it allows us to estimate parameters that are used to build an effective Anderson-Hubbard-type model Hamiltonian. The model is solved at the mean-field level, and the results are compared with the full DFT band structure to test the quality of the mapping. The model Hamiltonian is then used to study a *single* H impurity adsorbed on graphene, a situation that cannot be tackled with the current DFT-based methods and that allows us to identify in detail the structure of the induced defect as well as its magnetic properties without the complications generated by the interactions between impurities.

Within the single-impurity Anderson-Hubbard Hamiltonian, the mean-field approximation gives a magnetic solution for undoped graphene and a strong dependence of the impurity magnetic moment with doping—an effect with interesting implications for spintronics and for applications in magnetotransport devices.

In order to treat the delicate balance between kinetic energy and correlations at the defect including quantum fluctuations, we devised a minimal Anderson-Hubbard model that takes into account explicitly the electronic correlations at the impurity orbital as well as on the surrounding carbon atoms and replace the rest of the system with an effective medium.

An analysis of the isolated cluster illustrates the structure of the magnetic moment. For $-U_H < \varepsilon_H < 0$ and small hybridization V, the spin is localized at the H orbital while for large V, the spin is transferred to the carbon atoms forming a vacancylike state. For intermediate values of the hybridization that correspond to a realistic description of H, the stability region shows a neck, and the magnetic moment is in a linear combination of the impurity and C orbitals. The effect of the rest of the host graphene is treated as an effective medium with a pseudogap using the NRG. We consider the case of undoped graphene for which the Fermi energy lies at the Dirac point. As shown in Fig. 9, the region of stability of the magnetic moment is narrowed as the cluster is coupled to the rest of the system. This behavior can be understood in terms of the known results for the Anderson-impurity model in a system with a graphene like pseudogap. In the case of electron-hole symmetry, the spin is never screened[55] while away from the electron-hole symmetry, the spin can be screened at low temperatures if the Kondo coupling is larger than a critical value on the order of the bandwidth. Interestingly, within our model in the large-V regime (the vacancylike state), the electron-hole symmetry is recovered, and the magnetic moment remains unscreened.

While breaking the electron-hole symmetry will modify some of these results (a detailed study will be presented elsewhere), the main results of the present work are robust against it. (i) The spin is transferred to the carbon atoms as

the hybridization increases; (ii) the Kondo coupling can reach quite large values; and (iii) for realistic values of the parameters (obtained from our DFT calculations), the H-induced defect is halfway between the one corresponding to an adatom weakly coupled to pristine graphene and that of a carbon vacancy.

ACKNOWLEDGMENTS

We thank M. Vojta and T. Wehling for useful conversations. J.O.S. and A.S. acknowledge support from the Donors of the American Chemical Society Petroleum Research Fund and use of facilities at the Penn State Materials Simulation Center. G.U., P.S.C., A.D.H., and C.A.B. acknowledge financial support from PICTs Grants No. 06-483 and No. 2008-2236 from ANPCyT and PIP Grant No. 11220080101821 from CONICET, Argentina.

APPENDIX: NONINTERACTING SELF-ENERGY

In Sec. III we solved the adatom problem using a simplified model in which Coulomb interaction was assumed to be relevant only on the C_0 and C_n carbon atoms. In that case and if we are only interested in the properties of the reduced system formed by the adatom and the above mentioned C atoms, the presence of the rest of the graphene sheet can be taken into account through a self-energy contribution. In the following, we calculate this self-energy using the Dyson equation and taking advantage of the following facts. (i) The structure of the honeycomb lattice around a given atom has the same structure as that of a Bethe lattice (up to the second-nearest neighbors), allowing a simple disentanglement of the lattice Green function, and (ii) the exact lattice Green function of a given site $\mathcal{G}_i$ of the honeycomb lattice has an analytic closed form.[67]

Let us denote by $c^\dagger_\triangle = \sum_i c^\dagger_i/\sqrt{3}$ the fermionic operator that creates an electron in a state hat is a symmetric linear combination of the p_z orbitals of the three nearest-neighbor atoms of C_0. The quantity of interest is the noninteracting self-energy of that state $\Sigma_\triangle(\omega)$ due to the rest of the graphene (without C_0). That is, if $g_\triangle(\omega) = \langle\langle c_\triangle, c^\dagger_\triangle\rangle\rangle$ denotes the retarded Green function *in the absence* of the coupling with C_0, then $\Sigma_\triangle(\omega) = \omega - g^{-1}_\triangle(\omega)$. The Dyson equation $\boldsymbol{\mathcal{G}} = \boldsymbol{g} + \boldsymbol{g}\boldsymbol{V}\boldsymbol{\mathcal{G}}$ relates the unperturbed Green function $\boldsymbol{g}$ with the Green funtion $\boldsymbol{\mathcal{G}}$ in the presence of the perturbation $\boldsymbol{V}$. Taking the hopping between the site 0 and its three nearest-neighbors as the perturbation, we can immediately obtain the following expression for the Green function of the site 0 (corresponding to the p_z orbital of C_0):

$$\mathcal{G}_0 = g_0 + g_0 3t^2 \mathcal{G}_0 g_\triangle, \tag{A1}$$

where $g_0(\omega) = (\omega + i0^+)^{-1}$ and[68]

$$\mathcal{G}_0(\omega) = \frac{\omega}{2\pi t^2}\mathcal{S}\left(\frac{\omega^2 - 3t}{2t}\right)\mathcal{Q}\left(\frac{\omega^2 - 3t}{2t}\right) \tag{A2}$$

with

$$\mathcal{S}(x) = 8(\sqrt{2x+3} - 1)^{-\frac{3}{2}}(\sqrt{2x+3} + 3)^{-\frac{1}{2}}. \tag{A3}$$

Also,

$$\mathcal{Q}(x) = \begin{cases} K[k(x)^2] & \text{if } \mathrm{Im}(x)\mathrm{Im}(k) < 0, \\ K[k(x)^2] + 2ip(x)K[1 - k(x)^2] & \text{otherwise,} \end{cases} \tag{A4}$$

with $K(k)$ the complete elliptic integral of the first kind, $p(x) = \mathrm{sgn}[\mathrm{Im}(x)]$, and $k(x) = (2x+3)^{1/4}\mathcal{S}(x)/2$. After some straightforward algebra, we finally get

$$\Sigma_\triangle(\omega) = \omega - \frac{3t^2}{\Sigma_0(\omega)}, \tag{A5}$$

where $\Sigma_0(\omega) = \omega - \mathcal{G}^{-1}_0(\omega)$. We notice that in the low-energy limit ($|\omega| \to 0$),

$$-\mathrm{Im}[\Sigma_\triangle(\omega)] \simeq -3t^2\mathrm{Im}\,[\mathcal{G}_0(\omega)] = \sqrt{3}|\omega|. \tag{A6}$$

This shows that the effective density of states of the part of the graphene sheet that couples to the symmetric state defined above also presents a pseudogap and goes linearly to zero [see Fig. 10(a)].

A similar analysis can be done for the green function and the self-energy corresponding to the $|\pm\rangle$ states, $g_\pm(\omega)$ and $\Sigma_\pm(\omega)$, respectively. We then obtain

$$g_\pm(\omega) = \frac{3}{2}\mathcal{G}_0(\omega) - \frac{1}{2}\mathcal{G}_\triangle(\omega) \tag{A7}$$

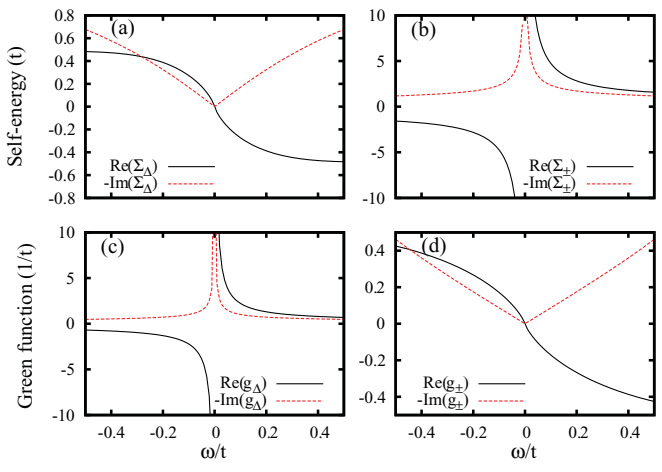

FIG. 10. (Color online) Self-energy and unperturbed Green functions of the C_n atoms. (a) and (c) correspond to the state $|\triangle\rangle$ while (b) and (d) correspond to the $|\pm\rangle$ states. Note that $\Sigma_\triangle(\omega)$ presents a pseudogap close to the Dirac point, and then $g_\triangle(\omega)$ shows resonantlike behavior (a vacancy state). The opposite behavior is observed for $\Sigma_\pm(\omega)$ and $g_\pm(\omega)$.

and

$$\Sigma_{\pm}(\omega) = \omega - g_{\pm}^{-1}(\omega) \tag{A8}$$

with $\mathcal{G}_{\triangle}(\omega) = [\omega - \Sigma_{\triangle}(\omega) - 3t^2 g_0(\omega)]^{-1}$. These functions are plotted in Figs. 10(b) and 10(d).

From these results, it is clear that at low energies, the $|\triangle\rangle$ state is only weakly coupled to the rest of the graphene sheet (excluding C_0) while the opposite is true for the other two orthogonal states $|\pm\rangle$, justifying our simplified model described in Sec. III.

[1] K. S. Novoselov, A. K. Geim, S. V. Morozov, D. Jiang, M. I. Katsnelson, I. V. Grigorieva, S. V. Dubonos, and A. A. Firsov, Nature (London) **438**, 197 (2005).

[2] M. I. Katsnelson, K. S. Novoselov, and A. K. Geim, Nat. Phys. **2**, 620 (2006).

[3] K. S. Novoselov, Z. Jiang, Y. Zhang, S. V. Morozov, H. L. Stormer, U. Zeitler, J. C. Maan, G. S. Boebinger, P. Kim, and A. K. Geim, Science **315**, 1379 (2007).

[4] A. K. Geim and K. S. Novoselov, Nat. Mater. **6**, 183 (2007).

[5] A. H. Castro Neto, F. Guinea, N. M. R. Peres, K. S. Novoselov, and A. K. Geim, Rev. Mod. Phys. **81**, 109 (2009), and references therein.

[6] S. Das Sarma, S. Adam, E. H. Hwang, and E. Rossi, Rev. Mod. Phys. **83**, 407 (2011).

[7] K. S. Novoselov, A. K. Geim, S. V. Morozov, D. Jiang, Y. Zhang, S. V. Dubonos, I. V. Grigorieva, and A. A. Firsov, Science **306**, 666 (2004).

[8] Y. Zhang, Y.-W. Tan, H. L. Stormer, and P. Kim, Nature (London) **438**, 201 (2005).

[9] P. R. Wallace, Phys. Rev. **71**, 622 (1947).

[10] P. O. Lehtinen, A. S. Foster, A. Ayuela, A. Krasheninnikov, K. Nordlund, and R. M. Nieminen, Phys. Rev. Lett. **91**, 017202 (2003).

[11] E. J. Duplock, M. Scheffler, and P. J. D. Lindan, Phys. Rev. Lett. **92**, 225502 (2004).

[12] J. C. Meyer, C. O. Girit, M. F. Crommie, and A. Zettl, Nature (London) **454**, 319 (2008).

[13] K. T. Chan, J. B. Neaton, and M. L. Cohen, Phys. Rev. B **77**, 235430 (2008).

[14] B. Uchoa, V. N. Kotov, N. M. R. Peres, and A. H. Castro Neto, Phys. Rev. Lett. **101**, 026805 (2008).

[15] A. H. Castro Neto and F. Guinea, Phys. Rev. Lett. **103**, 026804 (2009).

[16] D. W. Boukhvalov, M. I. Katsnelson, and A. I. Lichtenstein, Phys. Rev. B **77**, 035427 (2008).

[17] D. W. Boukhvalov and M. I. Katsnelson, J. Phys.: Condens. Matter **21**, 344205 (2009).

[18] A. Castro Neto, V. Kotov, J. Nilsson, V. Pereira, N. Peres, and B. Uchoa, Solid State Commun. **149**, 1094 (2009).

[19] P. S. Cornaglia, G. Usaj, and C. A. Balseiro, Phys. Rev. Lett. **102**, 046801 (2009).

[20] T. O. Wehling, M. I. Katsnelson, and A. I. Lichtenstein, Phys. Rev. B **80**, 085428 (2009).

[21] T. O. Wehling, A. V. Balatsky, M. I. Katsnelson, A. I. Lichtenstein, and A. Rosch, Phys. Rev. B **81**, 115427 (2010).

[22] T. O. Wehling, H. P. Dahal, A. I. Lichtenstein, M. I. Katsnelson, H. C. Manoharan, and A. V. Balatsky, Phys. Rev. B **81**, 085413 (2010).

[23] Z. M. Ao and F. M. Peeters, Appl. Phys. Lett. **96**, 253106 (2010).

[24] A. D. Hernández-Nieves, B. Partoens, and F. M. Peeters, Phys. Rev. B **82**, 165412 (2010).

[25] K. T. Chan, H. Lee, and M. L. Cohen, Phys. Rev. B **84**, 165419 (2011).

[26] N. Tombros, C. Jozsa, M. Popinciuc, H. T. Jonkman, and B. J. van Wees, Nature (London) **448**, 571 (2007).

[27] O. V. Yazyev and M. I. Katsnelson, Phys. Rev. Lett. **100**, 047209 (2008).

[28] M. Wimmer, İ. Adagideli, S. Berber, D. Tománek, and K. Richter, Phys. Rev. Lett. **100**, 177207 (2008).

[29] G. Usaj, Phys. Rev. B **80**, 081414(R) (2009).

[30] D. Soriano, F. Muñoz-Rojas, J. Fernández-Rossier, and J. J. Palacios, Phys. Rev. B **81**, 165409 (2010).

[31] C. Józsa, M. Popinciuc, N. Tombros, H. T. Jonkman, and B. J. van Wees, Phys. Rev. B **79**, 081402 (2009).

[32] W. Han, K. Pi, K. M. McCreary, Y. Li, J. J. I. Wong, A. G. Swartz, and R. K. Kawakami, Phys. Rev. Lett. **105**, 167202 (2010).

[33] O. V. Yazyev and L. Helm, Phys. Rev. B **75**, 125408 (2007).

[34] J. J. Palacios, J. Fernández-Rossier, and L. Brey, Phys. Rev. B **77**, 195428 (2008).

[35] O. V. Yazyev, Phys. Rev. Lett. **101**, 037203 (2008).

[36] R. Balog, B. Jørgensen, J. Wells, E. Lægsgaard, P. Hofmann, F. Besenbacher, and L. Hornekær, J. Am. Chem. Soc. **131**, 8744 (2009).

[37] O. V. Yazyev, Rep. Prog. Phys. **73**, 056501 (2010).

[38] P. Haase, S. Fuchs, T. Pruschke, H. Ochoa, and F. Guinea, Phys. Rev. B **83**, 241408 (2011).

[39] S. Casolo, O. M. Løvvik, R. Martinazzo, and G. F. Tantardini, J. Chem. Phys. **130**, 054704 (2009).

[40] D. C. Elias, R. R. Nair, T. M. G. Mohiuddin, S. V. Morozov, P. Blake, M. P. Halsall, A. C. Ferrari, D. W. Boukhvalov, M. I. Katsnelson, A. K. Geim, and K. S. Novoselov, Science **323**, 610 (2009).

[41] V. M. Pereira, F. Guinea, J. M. B. Lopes dos Santos, N. M. R. Peres, and A. H. Castro Neto, Phys. Rev. Lett. **96**, 036801 (2006).

[42] J.-H. Chen, L. Li, W. G. Cullen, E. D. Williams, and M. S. Fuhrer, Nat. Phys. **7**, 535 (2011).

[43] There is, however, some controversy in the literature regarding whether the value of U_C is closer to the critical value that would generate a magnetic instability in pure graphene.[69] Within the context of DFT, we used the QUANTUM EXPRESSO package[70] to obtain $U_C \sim 3.2$–3.5 eV.

[44] G. Kresse and J. Furthmüller, Comput. Mater. Sci. **6**, 15 (1996); Phys. Rev. B **54**, 11169 (1996).

[45] P. E. Blöchl, Phys. Rev. B **50**, 17953 (1994).

[46] G. Kresse and D. Joubert, Phys. Rev. B **59**, 1758 (1999).

[47] J. P. Perdew, K. Burke, and M. Ernzerhof, Phys. Rev. Lett. **77**, 3865 (1996).

[48] J. P. Perdew, K. Burke, and M. Ernzerhof, Phys. Rev. Lett. **78**, 1396 (1997).

[49]J. Neugebauer and M. Scheffler, Phys. Rev. B **46**, 16067 (1992); G. Makov and M. C. Payne, *ibid.* **51**, 4014 (1995).

[50]For the case of doped cells, the compensating charges are represented by a jellium. This approximation does not alter significantly the adsorption energies or the electronic structure of the system. In the real device geometry, charge is transferred to and from graphene through the electrodes. The compensating charges, in this case, are located in the region of the heavily doped silicon, separated from graphene by the insulating layer of SiO_2 that is typically of about 300 nm. For this geometry, modeling the neutralizing charge as a uniform background is quite close to the real device. To test this hypothesis, we noticed that for the distance from the graphene plane to the hydrogen atom in the top position, the change in electrostatic potential upon charging is minimal. This indicates that the charging effects do not create spurious electric fields at the position of the impurity. Consequently, the charging of the cell with the background correction reproduces well the effect of the field-effect transistor on this sample.

[51]J. O. Sofo, A. M. Suarez, G. Usaj, P. S. Cornaglia, A. D. Hernández-Nieves, and C. A. Balseiro, Phys. Rev. B **83**, 081411 (2011).

[52]N. M. R. Peres, F. Guinea, and A. H. Castro Neto, Phys. Rev. B **73**, 125411 (2006).

[53]J. Schrieffer and P. Wolff, Phys. Rev. **149**, 491 (1966).

[54]D. Withoff and E. Fradkin, Phys. Rev. Lett. **64**, 1835 (1990).

[55]L. Fritz and M. Vojta, Phys. Rev. B **70**, 214427 (2004).

[56]D. Jacob and G. Kotliar, Phys. Rev. B **82**, 085423 (2010).

[57]K. Ingersent, Phys. Rev. B **54**, 11936 (1996).

[58]M. Vojta, L. Fritz, and R. Bulla, Europhys. Lett. **90**, 27006 (2010).

[59]R. Bulla, T. Pruschke, and A. C. Hewson, J. Phys.: Condens. Matter **9**, 10463 (1999).

[60]K. Chen and C. Jayaprakash, J. Phys.: Condens. Matter **7**, L491 (1999).

[61]L. Fritz, S. Florens, and M. Vojta, Phys. Rev. B **74**, 144410 (2006).

[62]M. Vojta and L. Fritz, Phys. Rev. B **70**, 094502 (2004).

[63]B. Uchoa, T. G. Rappoport, and A. H. Castro Neto, Phys. Rev. Lett. **106**, 016801 (2011).

[64]C. Gonzalez-Buxton and K. Ingersent, Phys. Rev. B **57**, 14254 (1998).

[65]K. Wilson, Rev. Mod. Phys. **47**, 773 (1975).

[66]R. Bulla, T. A. Costi, and T. Pruschke, Rev. Mod. Phys. **80**, 395 (2008).

[67]T. Horiguchi, J. Math. Phys. (Melville, NY, US) **13**, 1411 (1972).

[68]Here, it is understood that $\mathcal{G}_0$ is evaluated with an infinitesimal imaginary part $\mathcal{G}_0(\omega + i0^+)$.

[69]T. O. Wehling, E. Şaşıoğlu, C. Friedrich, A. I. Lichtenstein, M. I. Katsnelson, and S. Blügel, Phys. Rev. Lett. **106**, 236805 (2011).

[70]M. Cococcioni and S. de Gironcoli, Phys. Rev. B **71**, 035105 (2005).